

Preliminary results of an in-beam PET prototype for proton therapy

F. Attanasi^a, N. Belcari^a, M. Camarda^a, G.A.P. Cirrone^b, G. Cuttone^b, A. Del Guerra^a,
F. Di Rosa^b, N. Lanconelli^c, V. Rosso^{a,*}, G. Russo^b, S. Vecchio^a

^aDepartment of Physics, University of Pisa and INFN Sezione di Pisa, Pisa, Italy

^bINFN Laboratori Nazionali del Sud, Catania, Italy

^cDepartment of Physics, University of Bologna and INFN Sezione di Bologna, Bologna, Italy

Available online 21 March 2008

Abstract

Proton therapy can overcome the limitations of conventional radiotherapy due to the more selective energy deposition in depth and to the increased biological effectiveness. Verification of the delivered dose is desirable, but the complete stopping of the protons in patient prevents the application of electronic portal imaging methods that are used in conventional radiotherapy. During proton therapy β^+ emitters like ^{11}C , ^{15}O , ^{10}C are generated in irradiated tissues by nuclear reactions. The measurement of the spatial distribution of this activity, immediately after patient irradiation, can lead to information on the effective delivered dose. First, results of a feasibility study of an in-beam PET for proton therapy are reported. The prototype is based on two planar heads with an active area of about $5 \times 5 \text{ cm}^2$. Each head is made up of a position sensitive photomultiplier coupled to a square matrix of same size of LYSO scintillating crystals ($2 \times 2 \times 18 \text{ mm}^3$ pixel dimensions). Four signals from each head are acquired through a dedicated electronic board that performs signal amplification and digitization. A 3D reconstruction of the activity distribution is calculated using an expectation maximization algorithm. To characterize the PET prototype, the detection efficiency and the spatial resolution were measured using a point-like radioactive source. The validation of the prototype was performed using 62 MeV protons at the CATANA beam line of INFN LNS and PMMA phantoms. Using the full energy proton beam and various range shifters, a good correlation between the position of the activity distal edge and the thickness of the beam range shifter was found along the axial direction.

© 2008 Elsevier B.V. All rights reserved.

PACS: 87.53.Jw; 87.53.Bn; 87.57.uk

Keywords: Proton therapy; Dosimetry; Positron emission tomography

1. Introduction

In tumor treatment, the therapeutic effectiveness of conventional electromagnetic radiation is intrinsically limited by its physical and radiobiological properties: heavy charged particles, like protons, can overcome these limitations due to the more selective energy deposition in depth and to an increased biological effectiveness [1–3].

The in-beam positron emission tomography (PET) is a proposed technique for the monitoring of heavy charged particles therapy [4–7]. In fact, the complete stopping of the ions inside the irradiated volume prevents the application

of electronic portal imaging methods used in conventional radiotherapy [8].

The in-beam PET is based on the imaging of the β^+ activity distributions induced in the target volume by the incident protons; β^+ emitters radioisotopes like ^{11}C , ^{15}O , ^{10}C are produced from their stable isotopes present in the irradiated volume, and the two 511 keV γ -rays from the β^+ e^- annihilation are then detected in coincidence by two appropriate detection heads.

An in situ measurement allows one to acquire the maximum statistics by detecting also the activity contribution by the very short half-life isotopes (e.g., ^{15}O), and to minimize blurring effects due to patient shifts during the transport to a clinical PET system.

A prototype of an in-beam PET system with a limited active area was realized and tested using the 62 MeV

*Corresponding author. Tel.: +39 050 2214 230; fax: +39 050 2214 317.
E-mail address: valeria.rosso@pi.infn.it (V. Rosso).

protons at the CATANA beam line in Catania, at the Istituto Nazionale di Fisica Nucleare-Laboratori Nazionali del Sud, where ocular pathologies are treated with the proton beam [9]. Cylindrical polymethylmethacrylate (PMMA) phantoms were used.

2. Materials and methods

The in-beam PET tomographic prototype is based on two planar heads, with an active area of about $5 \times 5 \text{ cm}^2$. Each head is made up of a squared position sensitive photomultiplier (Hamamatsu H8500) coupled to a matrix of LYSO scintillating crystals, manufactured by Hilger Crystals.

Each photomultiplier has 8×8 anodes for an active area of $49 \times 49 \text{ mm}^2$. The anode pitch is 6.08 mm, due to the anode size of $5.8 \times 5.8 \text{ mm}^2$ and the 0.28 inter-anode spacing.

To reduce the number of collected signals, a position encoding readout was implemented: first, a charge division circuit based on a symmetric charge division scheme connects each anode to any other belonging to the same row and column, so that only $8+8$ signals have to be amplified [10]. Then the eight signals, corresponding to the eight rows (X), after being amplified, are connected to each other with a resistive chain: finally, only the two extreme signals have to be acquired [11]. The X coordinate of the light spot is calculated by a standard algorithm: $X = (X_1 - X_2)/(X_1 + X_2)$. The same is done for the eight columns signals (Y). In this way only four signals from each head have to be acquired. The digitization of the four signals is performed on the acquisition board by ADCs, and then the data are transferred to a local PC via USB2 connection. The maximum count rate handled by the acquisition system is about 50 kHz in coincidence and 200 kHz events in single for each head.

A matrix of LYSO crystals ($2 \times 2 \times 18 \text{ mm}^3$ pixel dimensions) was used as scintillating material and was connected to the H8500 photomultiplier. The 23×23 pixels are separated by white epoxy creating an inter-pixel space of about $150 \mu\text{m}$: the final dimension of the crystals matrix is $4.9 \times 4.9 \text{ cm}^2$. The length of the crystals, 18 mm, was chosen so as to have 1.5 attenuation lengths at 511 keV.

In Fig. 1, the two detection heads and the acquisition board of the tomographic prototype are shown.

The photomultipliers, being sensible to daylight, were inserted inside a PVC cylindrical holder and then each one was fixed to an aluminum support. It is possible to change the distance between the heads: we chose to work at a distance of 14 cm in a symmetric configuration with respect to the phantom.

As explained above, for each γ interaction in each scintillating matrix $4+4$ digitalized signals are acquired and have to be processed before the reconstruction algorithm produces the 3D image of the activity distribution.

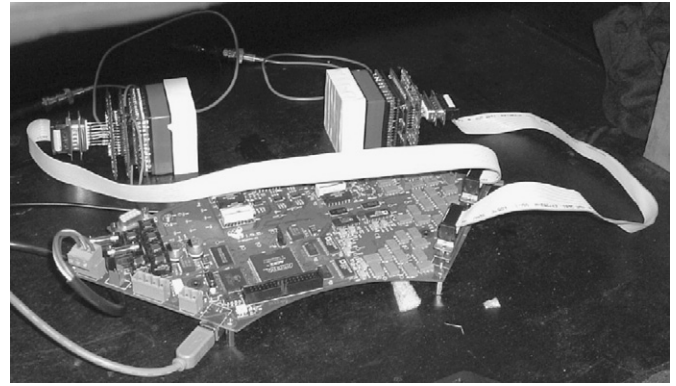


Fig. 1. The tomographic prototype: each head begins with the LYSO matrix, well visible wrapped with white Teflon tape, and attached to the photomultiplier. The resistive chain, after each photomultiplier, is then connected to the electronic board through a flat cable. An USB cable brings the data to a PC for the acquisition.

A specific calibration procedure is applied that takes into account anode gain and light yield variations; then the energy peak position of each pixel spectrum is determined by software and the required factor is applied [12]. After this procedure, the γ interaction coordinates, and the corresponding released energy in the crystal, are used by the reconstruction algorithm.

The iterative reconstruction algorithm, is based on an expectation maximization algorithm, and produces a 3D image of the activity distribution [13]. However, such a detected activity is not directly proportional to the delivered dose, because of the different nature of the physical processes that determine the β^+ activation and the energy deposition within the medium. Nevertheless, experimental results show that the distal dose fall-off is well correlated with the activity distal edge. This correlation is due to the threshold nature of the activation processes that determines the fall-off of the corresponding cross-section at energies approaching the Bragg peak. As a consequence, information about the beam range can be extracted by the distal edge of the activity distribution.

The aim of this work is to assess the PET prototype characteristics in terms of imaging capabilities, energy and spatial resolution and sensitivity; moreover, its performances with proton beams were measured.

3. Results

3.1. Imaging performances

To evaluate the imaging capabilities of the system, a ^{22}Na source was used.

For each detection head, flood field irradiation images were collected and a typical image is reported in Fig. 2.

In this image, all the pixels are well separated. The non-linearity reproduces the anode structure of the photomultiplier. This is due to the different sampling between the anode and the LYSO crystal: the anodes pitch is almost three times the crystals pitch. In order to obtain a good



Fig. 2. Flood field ^{22}Na irradiation image. 21×21 pixels are well visible.

separation between the pixels, also close to the border, the photomultiplier active area was reduced: a black tape shielded the LYSO pixels at the edges of the matrix that could introduce artifacts. The final useful LYSO matrix dimension is 21×21 crystals.

3.2. Energy resolution

After applying to the acquired data the correction procedures, as described in Section 2, the spectrum for each head is obtained. A lower energy threshold of about 80 keV was applied during all the acquisitions to eliminate electronic noise. The lutetium in LYSO contains a percentage of ^{176}Lu , a naturally occurring radioisotope with a half-life in the order of 4×10^{10} years.

In Fig. 3 are reported the obtained spectra for the LYSO matrix with and without the ^{22}Na source. The 202 and 307 keV γ emissions of ^{176}Lu radiation spectrum are very well visible, while the 401 keV γ emission causes a small bump in the fall-off of the spectrum. These background radiation energy emissions, together with the 511 keV line, were used to calibrate the energy response of our detection system. The data are reported in Fig. 4 showing the very good linearity of the system.

3.3. Spatial resolution

To evaluate the spatial resolution, a ^{22}Na point source was positioned at the center of the field of view of the tomographic prototype. The acquired data were analyzed at two different energy thresholds: a lower one to use all the events, also those that can arise from a casual coincidence generated from the ^{176}Lu emissions, and a

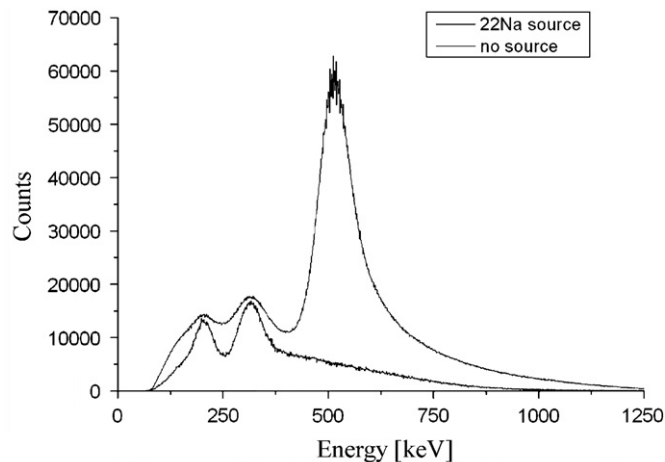


Fig. 3. Detection head energy spectra: the lower one corresponds to the background spectrum due to the presence of ^{176}Lu in the LYSO matrix; the upper one is the spectrum acquired for a flood field ^{22}Na irradiation. In the upper spectrum, the 511 keV γ peak together with the ^{176}Lu peaks are well identifiable.

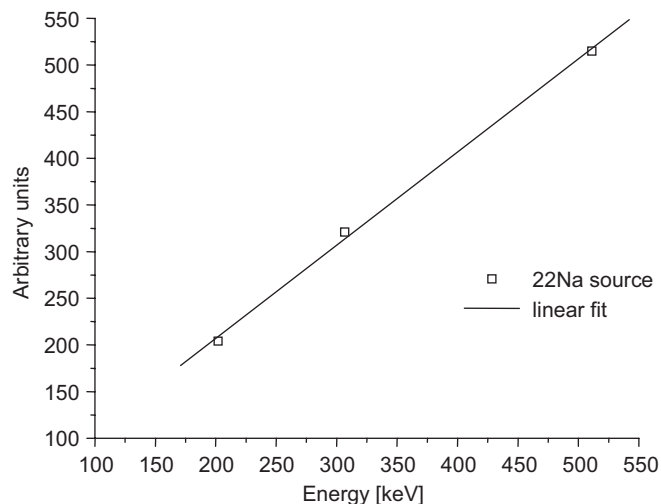


Fig. 4. DAC-arbitrary-units calibration curve vs. γ energy in keV. The reported points were obtained fitting the ^{22}Na energy spectrum reported in Fig. 3.

higher one at 350 keV to eliminate the ^{176}Lu emissions. The spatial resolutions for the reconstructed point source images, evaluated as the FWHM, are reported in Table 1 and no difference was found for the two energy thresholds.

To evaluate the possible influence of a scattering material, the ^{22}Na radioactive source was positioned inside a PMMA cylindrical holder 7 cm in diameter and 7 cm long. The obtained spatial resolution did not show any appreciable variations with respect to the experimental settings without the PMMA holder.

3.4. Prototype sensitivity

The tomographic prototype sensitivity was evaluated using a ^{22}Na point source positioned at the center of the

Table 1

The tomographic prototype spatial resolution evaluated for two energy thresholds

Energy threshold (keV)	X/Z (mm)	Y (mm)
150	1.7	7.7
350	1.7	7.6

X/Z is the plane parallel to the crystal surfaces; Y is the direction perpendicular to crystal surfaces.

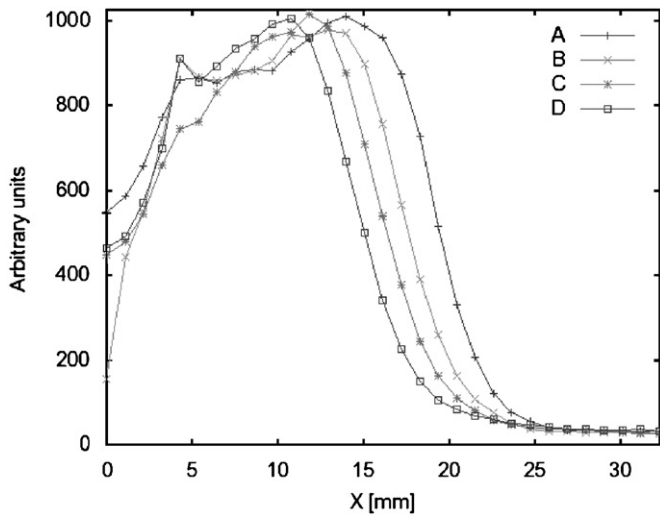


Fig. 5. Profiles of the positron depth activity profiles. Line A: no range shifter; line B: 2 mm PMMA; line C: 3.58 mm PMMA; line D: 5.4 mm PMMA.

field of view of the tomographic prototype. Applying a threshold of 150 keV, the sensitivity is 1%, while increasing this threshold at 350 keV the sensitivity decrease to 0.7%.

3.5. Depth activity profiles

To evaluate the capability of the tomographic prototype to appreciate different distal edges of the activity distributions, some PMMA phantoms were irradiated using different protons energy spectra, and the corresponding positron emitter distribution images were acquired.

The PMMA phantoms are cylinders with a diameter of 7 and 7 cm long. The PMMA cylinder axis was positioned aligned to the proton beam line (X direction).

The measurements were performed in a symmetric configuration of the tomographic prototype with a distance between the two heads set at 14 cm.

A mono-energetic 62 MeV proton beam and three different range shifters were used. The irradiation time was 1 min over the PMMA surface of 25 mm diameter.

Table 2

Comparison between the distances of two subsequent range shifters measured using the distal edges of the positron activity, and the corresponding difference between the PMMA thicknesses

Range shifter difference (mm)	2	1.6	1.8
Distal edge activity distance (mm)	1.9	1.4	1.4

A total dose of about 40 Gy was delivered during each irradiation. With an acquisition time of about 40 min after the end of each irradiation, the prototype provided about 10^5 coincidences on an irradiated volume of about 10 cm^3 .

The activity distributions were then calculated using the 3D iterative reconstruction algorithm [13]. Each image has a dimension of $42 \times 42 \times 130$ voxels. The central slices of four reconstructed longitudinal activity profiles (one without range shifter and the other three with increasing range shifters) are reported in Fig. 5.

A relative measurement was then performed: the distance between any two subsequent distal edges of the reconstructed activity profiles was evaluated and it is reported in Table 2.

Although the central slice activity images are extracted from low statistics 3D images, it was possible to appreciate differences in proton-induced activity distribution along the X direction (i.e., along the proton direction) lower than the 2 mm, i.e., smaller than the crystal pixel.

4. Conclusions

A compact tomographic prototype was realized and its spectroscopic, spatial and sensitivity characteristics were measured. The prototype was tested using 62 MeV protons. The obtained performances seem to be adequate for its use as an in-beam PET system for the measurements of the dose delivered during proton therapy if its sensitivity increases. A bigger prototype is now being constructed.

References

- [1] D.W. Miller, *Med. Phys.* 22 (1995) 1943.
- [2] M. Fuss, et al., *Int. J. Radiat. Oncol. Biol. Phys.* 49 (2001) 1053.
- [3] E.S. Gragoudas, et al., *Ophthalmology* 87 (1980) 571.
- [4] G.W. Bennett, et al., *Science* 200 (1978) 1151.
- [5] A. Del Guerra, et al., *Nucl. Instr. and Meth. A* 345 (1994) 379.
- [6] W. Enghardt, et al., *Nucl. Instr. and Meth. A* 525 (2004) 284.
- [7] K. Parodi, et al., *Med. Phys.* 34 (2007) 419M.
- [8] C.W. Hurkmans, et al., *Radiother. Oncol.* 58 (2001) 105.
- [9] G.A.P. Cirrone, et al., *IEEE Trans. Nucl. Sci.* NS-51 (3) (2004) 860.
- [10] P.D. Olcott, et al., *IEEE Trans. Nucl. Sci.* NS-52 (1) (2005) 21.
- [11] N. Belcari, et al., *Nucl. Instr. and Meth. A* 572 (2007) 335.
- [12] S. Vecchio, et al., *Nucl. Instr. and Meth. A* 569 (2006) 264.
- [13] A. Motta, et al., *Comput. Med. Imaging Graphics* 29 (2005) 587.